BAMS Article

# The Shortwave Spectral Radiometer for Atmospheric Science

## Capabilities and Applications from the ARM User Facility

Laura D. Riihimaki, Connor Flynn, Allison McComiskey, Dan Lubin, Yann Blanchard, J. Christine Chiu, Graham Feingold, Daniel R. Feldman, Jake J. Gristey, Christian Herrera, Gary Hodges, Evgueni Kassianov, Samuel E. LeBlanc, Alexander Marshak, Joseph J. Michalsky, Peter Pilewskie, Sebastian Schmidt, Ryan C. Scott, Yolanda Shea, Kurtis Thome, Richard Wagener, and Bruce Wielicki

**ABSTRACT:** Industry advances have greatly reduced the cost and size of ground-based shortwave (SW) sensors for the ultraviolet, visible, and near-infrared spectral ranges that make up the solar spectrum, while simultaneously increasing their ruggedness, reliability, and calibration accuracy needed for outdoor operation. These sensors and collocated meteorological equipment are an important part of the U.S. Department of Energy (DOE) Atmospheric Radiation Measurement (ARM) User Facility, which has supported parallel integrated measurements of atmospheric and surface properties for more than two decades at fixed and mobile sites around the world. The versatile capability of these ground-based measurements includes 1) rich spectral information required for retrieving cloud and aerosol microphysical properties, such as cloud phase, cloud particle size, and aerosol size distributions, and 2) high temporal resolution needed for capturing fast evolution of cloud microphysical properties in response to rapid changes in meteorological conditions. Here we describe examples of how ARM's spectral radiation measurements are being used to improve understanding of the complex processes governing microphysical, optical, and radiative properties of clouds and aerosol.

**KEYWORDS:** Aerosols; Cloud retrieval; Shortwave radiation; Instrumentation/sensors; Remote sensing; Surface observations

https://doi.org/10.1175/BAMS-D-19-0227.1
Corresponding author: Laura D. Riihimaki, laura.riihimaki@noaa.gov
Supplemental material: https://doi.org/10.1175/BAMS-D-19-0227.2

In final form 29 September 2020

**AFFILIATIONS: Riihimaki, Herrera, and Hodges**—CIRES, University of Colorado Boulder, and NOAA Global Monitoring Laboratory, Boulder, Colorado; **Flynn**—School of Meteorology, University of Oklahoma, Norman, Oklahoma; **McComiskey and Wagener**—Brookhaven National Laboratory, Upton, New York; **Lubin**—Scripps Institution of Oceanography, University of California, San Diego, La Jolla, California; **Blanchard**—ESCER Centre, Department of Earth and Atmospheric Sciences, University of Quebec at Montreal, Montreal, Quebec, Canada; **Chiu**—Colorado State University, Fort Collins, Colorado; **Feingold**—NOAA Chemical Sciences Laboratory, Boulder, Colorado Feldman—Lawrence Berkeley National Laboratory, Berkeley, California; **Gristey**—CIRES, University of Colorado Boulder, and NOAA Chemical Sciences Laboratory, Boulder, Colorado; **Kassianov**—Pacific Northwest National Laboratory, Richland, Washington; **LeBlanc**—Bay Area Environmental Research Institute, NASA Ames Research Center, Moffett Field, California; **Marshak and Thome**—NASA Goddard Space Flight Center, Greenbelt, Maryland; **Michalsky**—NOAA Global Monitoring Laboratory, Boulder, Colorado; **Pilewskie and Schmidt**—University of Colorado Boulder, Boulder, Colorado; **Scott, Shea, and Wielicki**—NASA Langley Research Center, Hampton, Virginia

In the decade before the U.S. Department of Energy (DOE) Atmospheric Radiation Measurement (ARM) facility was established in 1992, early modern climate models exhibited large differences in the climate response to doubling of atmospheric carbon dioxide (Ellingson et al. 2016). The primary drivers of the differences were the treatment of radiation transfer through the atmosphere and the representation of clouds and their interactions with solar and terrestrial radiation (Cess et al. 1990). The ARM Southern Great Plains (SGP) site was designed to examine cloud–radiation interactions through a strategically designed observational approach centered largely on active and passive remote sensing aimed at cloud properties, atmospheric state variables, and radiative fluxes distributed over a domain representative of climate model resolutions (Stokes 2016).

Since that time, the ARM suite of atmospheric radiation measurements has expanded and evolved with the focus of the science. While many original problems in atmospheric radiation have been addressed (Mlawer and Turner 2016; Mlawer et al. 2016), the climate forcing and feedbacks from cloud, aerosol, and cloud–aerosol interaction radiative effects remain some of the largest uncertainties in climate predictions (IPCC 2013). Improving predictability of the Earth system will require improved climate model parameterizations of the processes that impact concentrations and properties of these atmospheric constituents and their ultimate effect on radiative fluxes from regional to global scales. As climate models are on track to reach unprecedented resolution in the coming decade—3 km globally for the Simple Cloud Resolving E3SM Atmosphere Model (SCREAM) parameterizations within the DOE Energy Exascale Earth System Model (E3SM)—understanding the details of fine-scale processes that drive aerosol and cloud radiative effects over smaller domains and the manifestation of those processes at regional to global scales has come into focus.

Since its inception, the ARM User Facility has supported ground-based shortwave (SW) spectral measurements at its long-term fixed sites and field campaigns (Fig. 1a) in combination with a large suite of complementary instrumentation, including the aerosol observing system of in situ instruments (Uin et al. 2019) and the ARM radar network (Kollias et al. 2020), to improve understanding of atmospheric processes. These measurements are continually being tailored to provide increasingly detailed information of aerosol and cloud microphysical and optical properties that serve as the foundation for exploring the processes that introduce the largest uncertainties into climate predictions such as cloud phase, its impact on cloud formation, development, and radiative properties; cloud liquid water and its relationship to precipitation formation; and properties of aerosol and cloud in the clear–cloudy transition zone, the radiative effects of the transition zone, and their

(a)

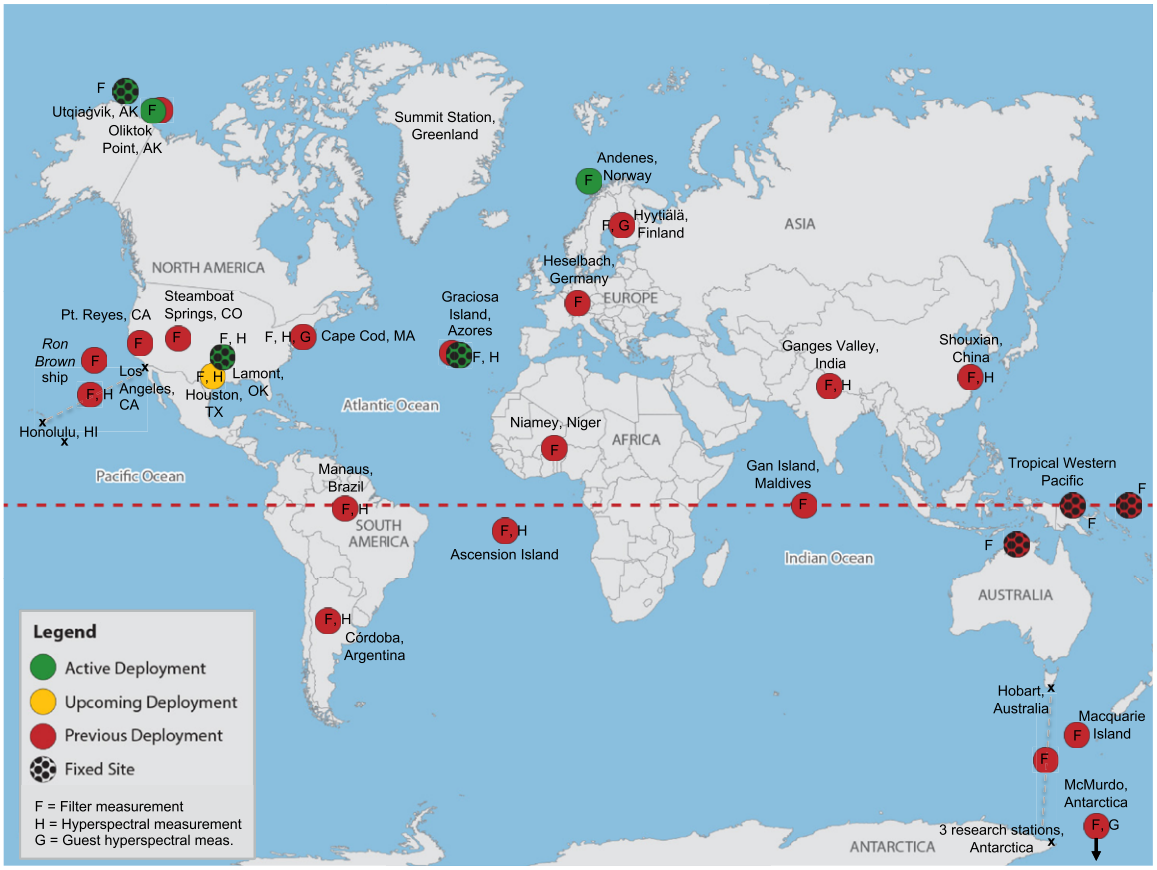


(b)

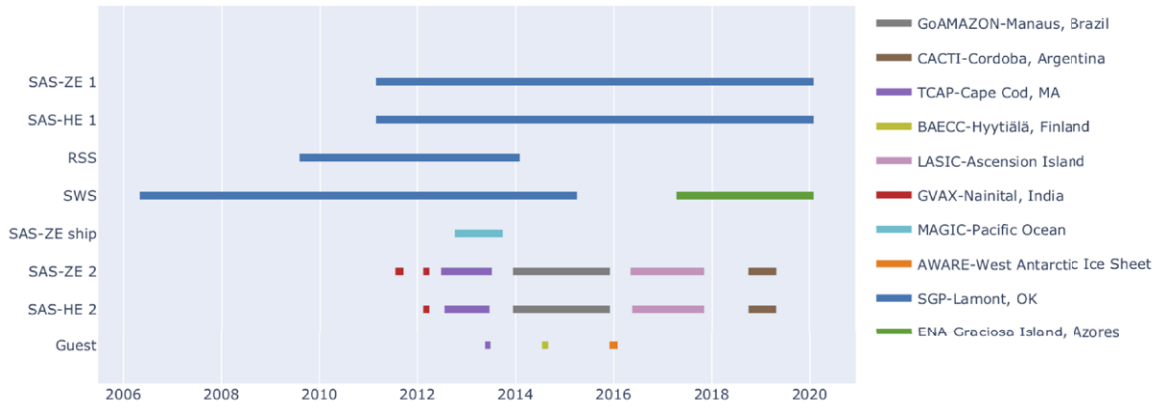


**Fig. 1. (a) Map of ARM deployments showing filter-based (F) or hyperspectral (H, G) SW spectral measurements. (b) Timeline of deployment of hyperspectral instruments at ARM campaigns, with campaign or site abbreviations and the name of locations given in the color bar. Any instrument deployed by a research group other than ARM is labeled as Guest. More details on instrument specifications are in Table 1. Note that the timeline shows when instruments were deployed but good data may not be available for the full campaign. More details about data quality can be found in section ES1 and on the ARM website.**

relationship to aerosol–cloud interactions in adjacent cloud fields. Here we describe current SW spectral radiation measurements made by ARM and review applications that are relevant to today's challenges in improving climate model representations of aerosols and clouds. These applications demonstrate the requirement for deployment of the most recent technology in SW spectral radiometric measurements in combination with ARM's extensive

suite of instrumentation to provide tools that can shed light on the next-generation challenges of aerosol and cloud radiative effects on climate.

## ARM's SW spectral radiation measurements and instrumentation

Solar radiation at the Earth's surface includes both direct transmitted and diffuse scattered components of SW radiation. The intensity and wavelength dependence of these radiation components depends intrinsically on the solar spectrum but also on the composition and structure of the atmosphere including gases, aerosols, and clouds. Spectral measurements of these components permit retrieval of cloud and aerosol properties, giving critical information about atmospheric properties and contributing to assessment of the Earth's radiation budget. Ground-based SW remote sensing has unique potential, particularly in concert with ARM's suite of other remote sensors, to retrieve high-temporal-resolution information about aerosol and cloud properties and their evolution, to capture detailed spatial features such as cloud edges, measurements of albedo and other surface properties, and to constrain radiative closure from the surface.

Spectrally resolved measurements of direct solar radiation and of hemispherically integrated diffuse scattered radiation incident on a horizontal plane are reported as *irradiance* with units of power per unit area per unit wavelength (e.g., W $m^{-2}$ $nm^{-1}$). When angularly resolved, the diffuse scattered spectral radiation is reported as *radiance* with units of power per unit area per unit wavelength per steradian. *Multispectral* instruments measure radiometric quantities in discrete spectral bands typically defined by narrowband interference filters, while *hyperspectral* instruments provide hundreds or thousands of contiguous measurements spanning a wide wavelength range.

ARM operates a collection of instruments using complementary techniques to measure different elements of shortwave spectral radiation. Sun-tracking sky-scanning photometers provide direct normal solar irradiance and angularly resolved sky *radiance*. Rotating shadowband radiometers provide components of radiation incident on a horizontal surface, thus direct horizontal solar irradiance and *diffuse hemispheric irradiance*. Downward-facing radiometers provide upwelling *hemispheric irradiance*. Narrow field-of-view (FOV) upward-facing radiometers provide high-temporal-resolution *zenith radiance*. Initially only multispectral narrowband instruments were routinely operated but starting in 2003 (and with an expansion in 2010) a variety of shortwave spectrometers have been deployed that provide routine hyperspectral measurements. A rich dataset of both multispectral and hyperspectral irradiance and radiance measurements now exists in the ARM data archive (e.g., Figs. 2 and 3; https://arm.gov/data) spanning the ultraviolet, visible, and SW near-infrared wavelengths (Table 1) with the unique potential to better understand cloud, aerosol, and radiation properties and processes. Each of these measurement types, whether multispectral or hyperspectral, hemispheric FOV or narrow FOV, or sun-tracking or shadowbanding, have their own strengths and weaknesses with increased benefits when used in concert.

***Using SW spectral hemispheric irradiance measurements for retrievals and radiative closure.*** The Multi-Filter Rotating Shadowband Radiometer (MFRSR; Harrison et al. 1994; Harrison and Michalsky 1994) incorporates a shadowband and a hemispheric diffuser to measure direct and diffuse hemispheric irradiance on a horizontal surface simultaneously at six spectral wavelengths (415, 500, 615, 676, 870, and 940 nm, see Fig. 2) and is deployed along with a downfacing Multi-Filter Radiometer (same as MFRSR but without the shadowband) for upwelling spectral irradiance at matched wavelengths. During the last 2.5 decades, a wide range of climate-relevant applications of MFRSR data were documented in numerous research articles and highlighted in several comprehensive reviews (e.g., McComiskey and Ferrare 2016; Turner et al. 2016; Michalsky and Long 2016). These

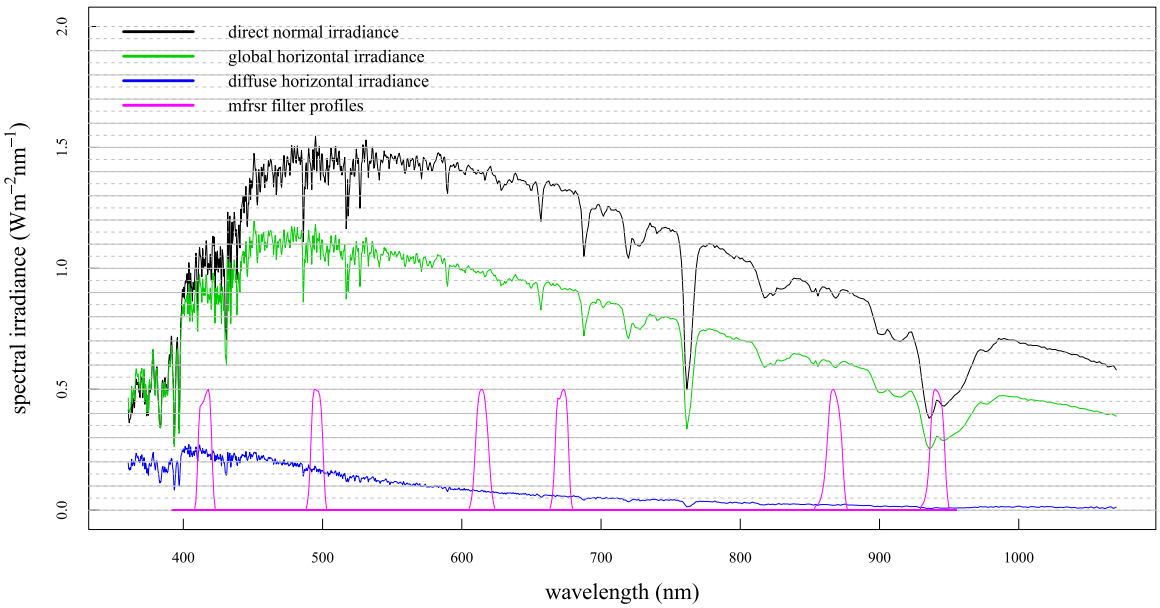


**Fig. 2. Cloud-free spectral irradiances as measured using the RSS. The spectral resolution is higher in the ultraviolet portion of the spectrum compared to the near-infrared. The nominal spectral positions and bandwidths of MFRSR filters are superimposed. More details on the specifications of the RSS and MFRSR can be found in Table 1.**

applications related to the atmospheric column include 1) a multiyear climatology of aerosol optical depth and Ångstrom exponent (Michalsky et al. 2010), 2) aerosol intensive properties like the single-scattering albedo and the asymmetry parameter (Kassianov et al. 2005, 2007; Ge et al. 2010), 3) total column precipitable water vapor (Michalsky et al. 1995; Alexandrov et al. 2009), 4) trace gases (Alexandrov et al. 2002a,b), 5) cloud optical depth (Min and Harrison 1996; Barnard et al. 2008), 6) cloud amount (Min et al. 2008; Kassianov et al. 2011a), and 7) assessment of the uncertainty in the radiative forcing of aerosols (McComiskey et al. 2008) and cumulus clouds (Kassianov et al. 2011b).

ARM has also deployed several shortwave spectrometers since the early 2000s (Fig. 1b) to measure hyperspectral irradiance (e.g., Fig. 2). The Rotating Shadowband Spectrometer (RSS) and Shortwave Array Spectroradiometer–Hemispheric (SASHe1 and SASHe2) systems provide hyperspectral analogs to the multispectral measurements of the MFRSR at the SGP and ARM Mobile Facility sites (Fig. 1b). The hyperspectral coverage (360–1,070 nm for RSS, 380–1,700 nm for SASHe) offers exciting potential for aerosol and cloud studies through the distinct quantification of the radiative impact of each atmospheric constituent and their unique spectral signatures. While the operation of these instruments can be operationally challenging, efforts are underway to define data epochs of hyperspectral measurements with known confidence, particularly for the infrared. Comparison of aerosol optical depths (AODs) retrieved from the RSS and SASHe measurements with concurrent AODs from the MFRSR and ARM Cimel sunphotometers (CSPHOTs) is an effective approach currently being pursued for identifying satisfactory operation and calibration of the hyperspectral instruments.

SW spectral irradiance measurements also provide the opportunity for new spectral closure experiments comparing measured and modeled spectral radiation, to improve the level of accuracy of atmospheric retrievals, radiative transfer models, and radiometric measurements, particularly in concert with the expected launch of the CLARREO Pathfinder (CPF) mission in 2023 (Wielicki et al. 2013). CPF will deliver hyperspectral measurements from the International Space Station, giving new potential to perform SW spectral closure experiments over ARM sites from the surface and top of atmosphere (TOA) simultaneously. The advent of

this mission has also led to new calibration technologies that could improve ground-based measurements (see details in section ES3 in the online supplemental material).

These closure activities can help evaluate novel retrieval developments. For example, it was recently shown that MFRSR data can be used to estimate the areal-averaged and spectrally resolved surface albedo under overcast skies (Kassianov et al. 2014, 2017; section ES4), conditions where you cannot observe albedo from satellites, which challenges TOA surface energy budget calculations (e.g., Stephens et al. 2012).

***Retrieving cloud properties using SW spectral radiance.*** The ARM CSPHOTs are part of the NASA Aerosol Robotic Network (AERONET) (Holben et al. 1998) and measure solar irradiance and narrow FOV radiances (Fig. 3, Table 1) following standard measurement protocols: direct sun, almucantar, and principal plane. The direct sun extinction gives an accurate measure of the column aerosol optical depth, and through the spectral deconvolution algorithm (SDA), a measure of fine-mode fraction. Assuming aerosols are distributed uniformly, the almucantar and principal plane sky radiance can be inverted to yield a number of other aerosol properties: particle size distribution; refractive index; asymmetry parameter; and when AOD is sufficiently large, absorption optical depth and single-scattering albedo (Dubovik and King, 2000; Giles et al. 2019).

In November 2004, the so-called "cloud mode" (Chiu et al. 2010, 2012) was added, which instead of parking the CSPHOT when the sun is blocked, points the instrument to the zenith to be used in cloud optical depth and effective radius retrievals. The cloud-mode observational strategy was largely motivated by the work using the ARM Narrow Field of View (NFOV) radiometer (Table 1) that measured zenith radiance at 673- and 870-nm wavelengths with 1-s time resolution (Marshak et al. 2004; Chiu et al. 2006).

The Shortwave Spectrometer (SWS) and Shortwave Array Spectroradiometer–Zenith (SASZe1 and SASZe2) provide hyperspectral zenith radiances at 1 Hz (Fig. 3). These instruments have operated at the SGP, the Azores, and selected ARM Mobile Facility sites (Fig. 1b). The broad spectral coverage and fast temporal sampling combined with a dynamic range able to measure both cloudy and cloud-free scenes make these instruments attractive to

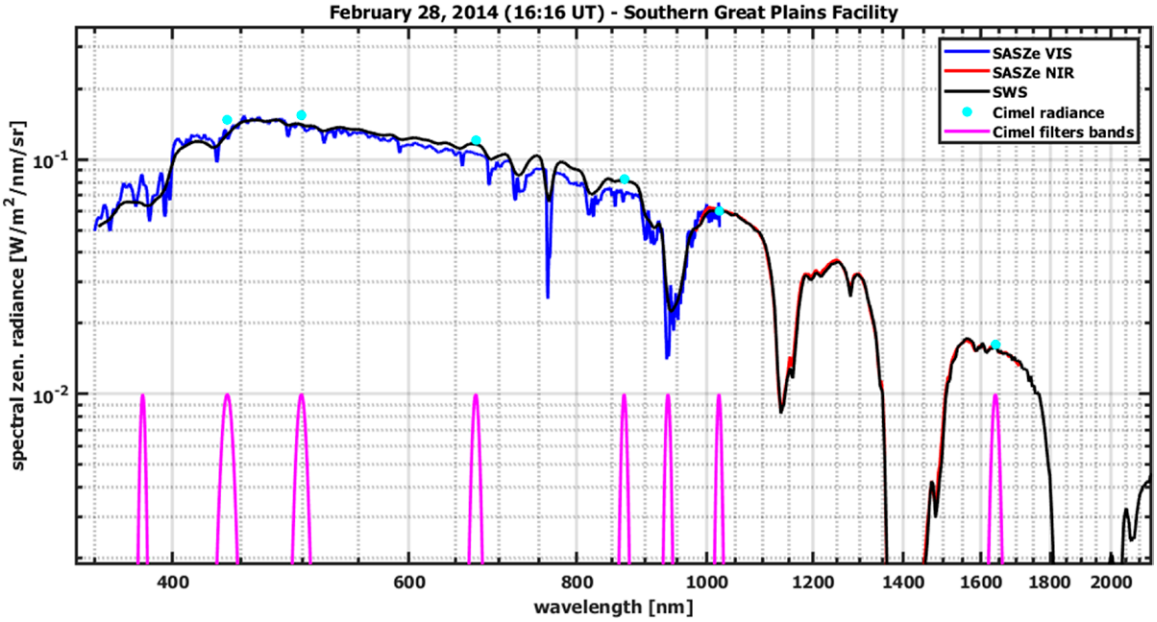


**Fig. 3. Spectral zenith radiances from cloudy skies as measured using the SWS (black) and the visible (blue) and near-infrared (red) spectrometers of the SASZe. Filter-based measurements from the CSPHOT are also shown along with the nominal spectral positions and bandwidths of CSPHOT filter.**

**Table 1. Filter-based and hyperspectral measurements fielded by the ARM program in at least one site or field campaign over the years. The "Date routine" column refers to the date when it was first made routine at SGP if that was its first site. The "Measurement" column uses abbreviations: irrad = hemispheric irradiance; dirh = direct horizontal irradiance; difh = diffuse horizontal irradiance; toth = total hemispheric downwelling irradiance; dirn = direct normal irradiance; rad = narrow FOV radiance. The "WL" column lists the wavelengths measured for filter-based measurements or the wavelength ranges for hyperspectral measurements. The "Comment, modes" column describes orientations, scanning strategies, FOV, or information about where the instruments were deployed for guest instruments. The final column gives a DOI or URL where data and documentation can be accessed if available.**

| Instrument | Date routine | Measurement | WL (nm) | Comment, modes | DOI or URL |
|---|---|---|---|---|---|
| MFR 10m | Mar 1994 | Upwelling irrad | 415, 500, 615, 673, 870, 940 | Upwelling hemispheric, 10-m tower, concurrent spectral measurements | 10.5439/1025224 |
| MFR 25m | Mar 1994 | Upwelling irrad | 415, 500, 615, 673, 870, 940 | Upwelling hemispheric, 25-m tower, concurrent spectral measurements | 10.5439/1025225 |
| MFRSR | Jan 1997 | dirh, difh, toth | 415, 500, 615, 673, 870, 940 | Shadowband with horizontal diffuser (no direct normal), concurrent spectral measurements | 10.5439/1034918 |
| CSPHOT | Mar 1998 | dirn, rad | 340, 380, 440, 500, 675, 870, 1,020, (1,640) | Direct normal solar, sky-scanning, cloud-zenith, 1,640 nm after Mar 2007, sequential spectral measurements. | www.arm.gov/capabilities/instruments/csphot |
| NIMFR | Aug 1997 | dirn | 415, 500, 615, 673, 870, 940 | Direct normal solar, concurrent spectral measurements | 10.5439/1025258 |
| NFOV | Mar 2000 | rad | 870 | 1.2° zenith | www.arm.gov/capabilities/instruments/nfov |
| NFOV2 | Sep 2004 | rad | 673, 870 | 1.2° zenith, moved to AMF1 after Nov 2006, two concurrent spectral measurements | 10.5439/1025257 |
| RSS105 | May 2003–Dec 2007 | dirh, difh, toth | Si (360–1,070) | Shadowband with horizontal diffuser (no direct normal), concurrent spectral measurements | 10.5439/1025267 |
| RSS | Aug 2009–Mar 2014 | dirh, difh, toth | Si (360.4–1,070.1) | Refurbished in 2009<br>1,002 pixels, spectral resolution varies from 0.6 nm at 360 to 7 nm at 1,070 | www.arm.gov/data/data-sources/rss-141 |
| SWS | May 2006 | rad | Si (350–1,000), InGaAs (970–2,200) | 1.4° zenith, moved to ENA in Apr 2016, concurrent spectral measurements | 10.5439/1025301 |
| SASHe | Mar 2011 | dirh, difh, toth | Si (350–1,000), InGaAs (970–1,700) | Shadowband with horizontal diffuser (no direct normal), concurrent spectral measurements | www.arm.gov/capabilities/instruments/sashe<br>10.5439/1150262<br>10.5439/1150263 |
| SASZe | Mar 2011 | rad | Si (350–1,000), InGaAs (970–1,700) | 1° zenith, concurrent spectral measurements | www.arm.gov/capabilities/instruments/sasze<br>10.5439/1025272<br>10.5439/1025273 |
| Aerodyne TWST | Guest instruments | rad | Si (350–1,000) | Aerodyne, Scott, AMF1 TCAP May–Jun 2013, AMF1 BAECC Jul–Aug 2014<br>Zenith radiance, concurrent spectral measurements | https://arm.gov/research/campaigns/amf2013fertcs<br>https://arm.gov/research/campaigns/amf2014baecc-twst |
| Panalytical FieldSpec Pro | Guest instruments | toth (flux) | Si (350–1,000), InGaAs (970–2,200) | Lubin, AWARE concurrent spectral measurements | Soon to be available on arm.gov |

studies of cloud properties and cloud–aerosol interactions. The narrow field of view also better matches the field of view of active sensors like lidars and vertically pointing cloud radars and passive sensors in the infrared and microwave, allowing for more consistent multi-instrument retrievals.

Operationally, these instruments have proven to be robust and reliable with very little down time. However, direct comparison of concurrent zenith radiance measurements, as

seen in Fig. 3, shows good agreement at some wavelengths and times, but at times can show discrepancies of up to 10%–20%, which exceeds the uncertainties of the calibration sources. Efforts are underway to make more comparisons such as these to better quantify uncertainties in the measurements, improve consistency between datasets, and determine potential instrument solutions such as more frequent onsite calibration, built-in light sources to identify wavelength-dependent changes, and developing vicarious calibration techniques.

A number of retrieval methodologies exist in the literature that use hyperspectral measurements to more accurately or flexibly retrieve cloud optical properties such as cloud optical depth and particle effective radius (section ES2). The impact of these measurement uncertainties varies by retrieval methodology, and in fact, many retrieval methodologies based on slopes (e.g., McBride et al. 2011) or the shape (LeBlanc et al. 2015) of the SW spectra mitigate challenges with absolute calibration accuracy, allowing more effective use of the spectral measurements. For example, the studies of the mixing zone between clear and cloudy skies described in the following section use retrievals of cloud optical depth and effective radius from multiple spectral zenith radiance instruments with absolute accuracy differences of 15%–20%, but these accuracy differences had little impact on the retrievals because ratios of cloudy and clear spectra are used (Yang et al. 2016, 2019; section ES5).

The following section describes examples of how some of these retrieval methodologies are beginning to be used in concert with the array of instrumentation at ARM sites to disentangle the microphysical processes impacting cloud radiative effects.

## Advances in understanding of cloud microphysical processes using ARM SW spectral measurements

***Shedding new light on high-latitude cloud processes.*** Shortwave spectral measurements have the potential to make significant contributions to atmospheric science at high latitudes. At remote field sites where aircraft in situ measurements are difficult, and where more advanced active remote sensors such as high-spectral-resolution lidar (HSRL) and cloud research radars are not available, spectral, near-infrared measurements of downwelling irradiance or zenith radiance provide valuable information about cloud microphysical properties and their influence on the surface radiation budget. In the near-infrared, radiation transmitted through clouds is sensitive to both the cloud thermodynamic phase and the effective droplet or ice particle size. Shortwave spectral irradiance measurements have shown how cloud ice water attenuates surface shortwave irradiance, relative to an equivalent liquid water cloud, in springtime Arctic stratus (Lubin and Vogelmann 2011), and how contrasting Antarctic meteorological regimes influence surface irradiance through varying cloud properties (Scott and Lubin 2014). The remote high latitudes are very data sparse, and even a modest deployment of spectral radiometric instruments can yield valuable case studies for process parameterization in climate modeling.

Figure 4 provides a demonstration of detecting polar cloud microphysical changes at high time resolution using shortwave spectral irradiance measurements. A Panalytical (Inc.) FieldSpec Pro Jr spectroradiometer measuring spectral irradiance over the interval 350–2,200 nm was deployed with the ARM West Antarctic Radiation Experiment (AWARE) at the West Antarctic Ice Sheet (WAIS) Divide Ice Camp (79°28′03″S, 112°05′11″W), in December 2015 and January 2016, and recorded data continuously in 1-min intervals (Wilson et al. 2018). Between 10 and 17 January AWARE sampled a major surface melting event (Nicolas et al. 2017) driven by significant increases in temperature and moisture in the lower troposphere over West Antarctica and the Ross Ice Shelf. This brought substantial variability in cloud microphysics alternating between mixed-phase and primarily liquid-phase clouds. In Fig. 4, the variability in the 1.6-$\mu$m spectral irradiance represents a transition in the low-level stratiform cloud deck between a mixed-phase and liquid phase [as described in Wilson et al. (2018)]. Under the

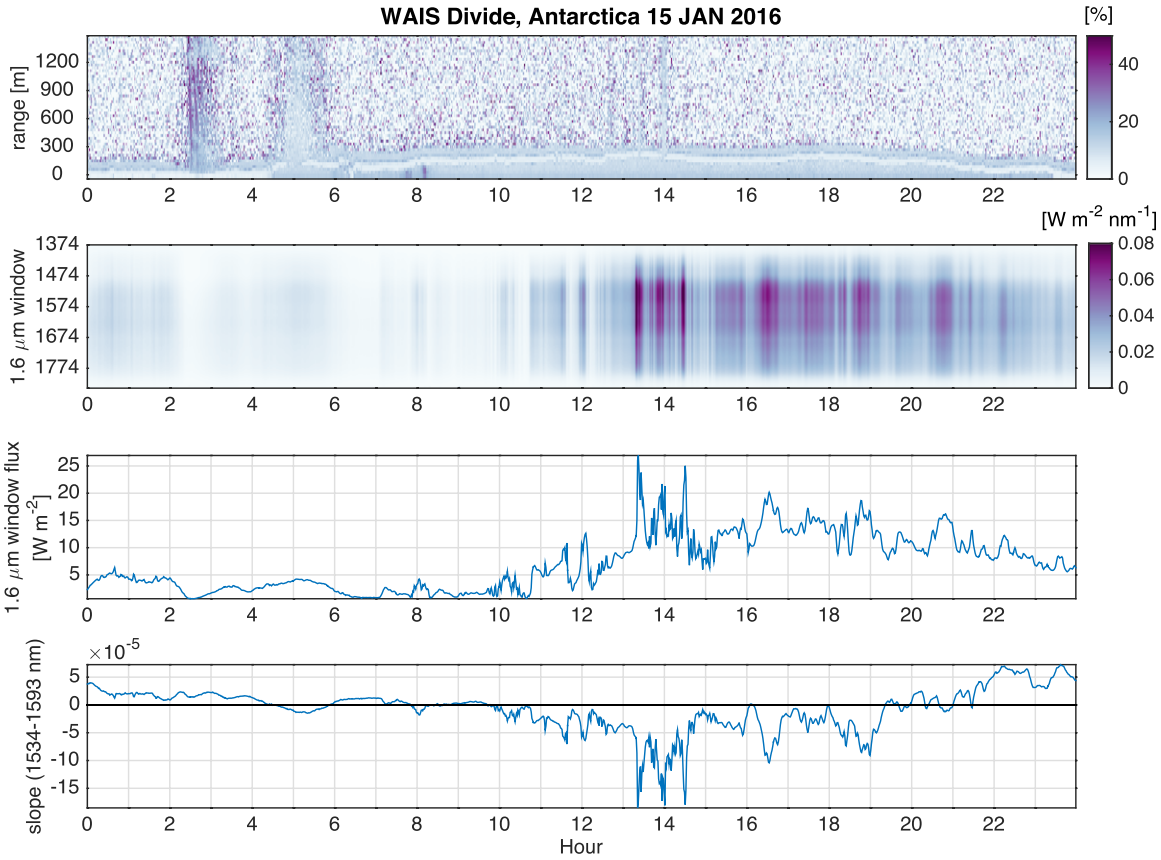


**Fig. 4. Evolution of 1.6-$\mu$m-window spectral irradiance throughout 15 Jan 2016 at WAIS Divide, Antarctica. Time given in hours UTC. (top) Micropulse lidar (MPL) depolarization ratio indicating nearly continuous low-level cloud cover. (bottom three panels) Irradiance spectrum recorded at 1-min intervals over the entire 1.6-$\mu$m window, the irradiance integrated over the window, and the slope of a linear fit through the spectral irradiance between 1,534 and 1,593 $\mu$m with a negative slope indicating liquid water.**

mainly liquid water cloud starting just after midday (UTC) the 1.6-$\mu$m-window downwelling irradiance increases by a factor of 3.

***Understanding precipitation formation in warm clouds.*** Process-level understanding of cloud and precipitation formation is key for addressing outstanding issues of warm clouds, such as climate model tendency to underestimate cloud fraction but overestimate cloud albedo for low-topped clouds (Nam et al. 2012); drizzling too lightly and too frequently (Stephens et al. 2010); and the large uncertainty in cloud feedbacks in models (Bony and Dufresne 2005; Klein and Hall 2015). Such understanding requires high-temporal-resolution and high-spatial-resolution observations to unravel or to validate. While active sensors like radar provide critical range-resolving measurements to capture structures of clouds and precipitation, radar is not independently capable of providing quantitative microphysical and optical properties. Shortwave radiation measurements obtained from instruments having comparable field of view with radar can be used alongside active sensors to better constrain retrieved quantities.

Combining shortwave zenith radiances at multiple wavelengths to retrieve cloud microphysical properties with scanning cloud radar measurements to give spatial context, Fielding et al. (2014) retrieved detailed three-dimensional (3D) fields of liquid water content and effective radius for nonprecipitating clouds. The capability of retrieving information from highly heterogeneous clouds (as shown in their cumulus case) not only helps achieve surface radiation closure, but also allows us to properly collect statistics of cloud populations. More

importantly, cloud evolution can be closely monitored for studying cloud transitions and their relation to the environment.

Using zenith spectral radiance measurements along with vertically pointing cloud radar and lidar, Fielding et al. (2015) showed that it is possible to retrieve cloud and drizzle properties simultaneously. An example from the ARM Eastern North Atlantic (ENA) site is shown in Fig. 5. This type of joint retrieval allows us to gain new insight into drizzle formation. For example, coincident cloud and in-cloud drizzle retrievals provide observational constraints on autoconversion and accretion processes (e.g., Mace et al. 2016). Observed cloud and drizzle spatial covariability can also be used to evaluate and improve cloud microphysics schemes in models (e.g., Boutle et al. 2014). Additionally, below-cloud drizzle is a key component to characterize drizzle evaporation and the subsequent impact on dynamics in the subcloud layer.

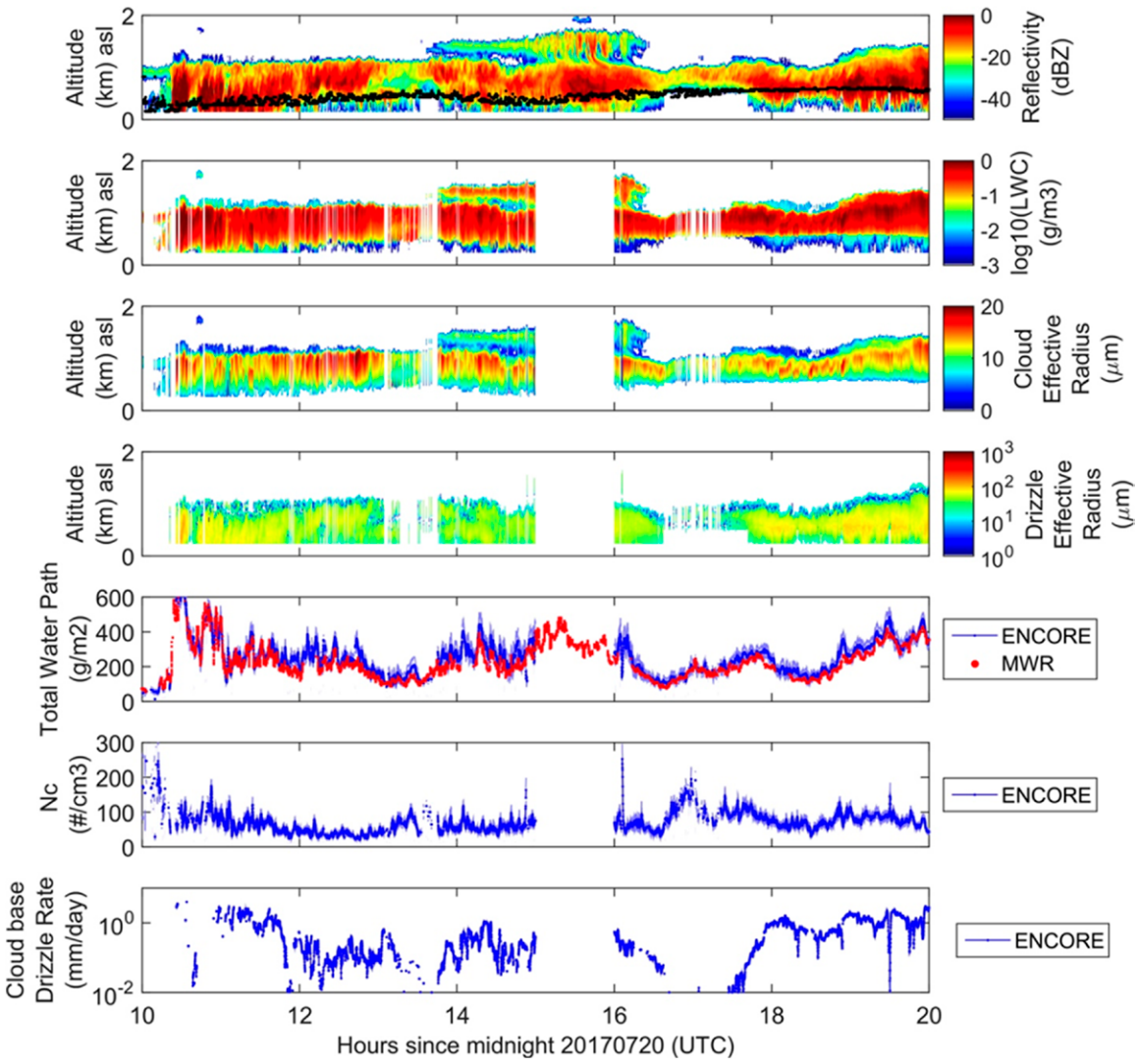


**Fig. 5. An example for retrieving properties of concurrent cloud and drizzle using combined measurements of cloud radar, lidar, and shortwave zenith radiance from the ARM Eastern North Atlantic site on 20 Jul 2017. Retrievals are based on an Ensemble Cloud Retrieval method (ENCORE). (top to bottom) Observed radar reflectivity with cloud-base height (black lines), retrieved water content, cloud effective radius, drizzle effective radius, total water path (i.e., the sum of the cloud and drizzle water path), cloud droplet number concentration, and cloud-base drizzle rate, respectively. For comparison, total water path from microwave radiometer observations is coplotted in the fifth panel (red). Note that retrievals for multilayer clouds at 1500–1600 UTC are not available since the assumption used in the retrieval method is likely violated.**

***Observing mixing and aerosol–cloud interactions in the transition zone.*** The transition zone between cloudy and clear air is a region of strong aerosol–cloud interaction where aerosol particles humidify and swell when approaching the cloud, while cloud drops evaporate and shrink when moving away from the cloud. The transition zone is also contaminated by "weak cloud elements," such as cloud fragments sheared off from adjacent clouds (Koren et al. 2007, 2009). Using satellite observations from CALIPSO, Varnai and Marshak (2011) showed that transition zones between clear and cloudy air are ubiquitous: about *half* of all clear-sky pixels over ocean are within 5 km of a low cloud (below 3-km altitude). This zone is more extensive than was previously thought (Bar-Or et al. 2010), and thus it complicates estimates of the aerosol indirect effect and aerosol radiative forcing—excluding aerosols near clouds will dramatically reduce the database and underestimate the forcing, while including them may overestimate the forcing because of unaccounted cloud contamination.

The 1-Hz-temporal-resolution data from the ARM shortwave spectrometers (Table 1: SASZe, SWS) provide a unique opportunity to study the transition zone as they capture the needed temporal and spatial resolution, which are difficult to measure from space-based or aircraft platforms. In addition, spectral radiative measurements help us study the factors controlling the entrainment and homogeneous versus inhomogeneous mixing processes.

By approximating the shortwave spectra in the cloud–clear transition zone as a linear combination of purely clear and purely cloudy spectra (see details in section ES5), we can characterize cloud optical thickness and cloud droplet effective radius in the transition zone. When applying this method to the measurements of a ground-based shortwave spectroradiometer in continental and maritime conditions (Yang et al. 2016, 2019), we found that cloud optical depth consistently decreases in both cases, while droplet size decreases much more substantially for the continental regime, suggesting different mixing processes for the two types of clouds. This is consistent with our theoretical understanding of the effect of relative humidity on the mixing types (Pinsky and Khain 2018).

## Progress and potential of SW Spectral measurements to observe and understand 3D radiative effects

New approaches that balance detailed process understanding with emergent phenomena in order to improve quantification of radiative effects in complex cloud–aerosol–radiation environments (Feingold et al. 2016) are required for advancing predictive modeling of the global climate. One such approach is to represent the irradiance field at a given level in the atmosphere as a probability density function (PDF) of downwelling irradiance (Schmidt et al. 2007, 2009), to reveal how different cloud field morphologies and aerosol conditions manifest in different radiation patterns at the Earth's surface. The PDF of aircraft observations (Fig. 6) at 500 nm acquired during the Gulf of Mexico Atmospheric Composition and Climate Study (GoMACCS) campaign (Lu et al. 2008) exhibited a distinct bimodal structure under shallow cumulus clouds (Schmidt et al. 2009), representing cloud shadows and the clear sky between clouds separately. The use of these detailed spectral measurements of the complex cloud field allows for attribution of radiative effects to the different components of the system.

This bimodal structure of the irradiance PDF can also be captured by multifilter radiometers that are more widely deployed, providing improved spatial sampling. The MFRSR makes continuous measurements at the SGP central facility and several extended facilities within approximately 75 km of the central facility (ARM 2019). MFRSR irradiance at 500 nm under shallow cumulus clouds from the central facility (Figs. 7a,b) provides limited statistics, making the PDF shape difficult to quantify (Fig. 7a). However, observations across ten sites produce a PDF that is more distinct and robust (Fig. 7b). Large-eddy simulations (LESs) informed by observations (Gustafson et al. 2020) were used to reproduce the cloud field for radiative transfer (RT) modeling of this case. One-dimensional (1D) RT, which models the atmosphere

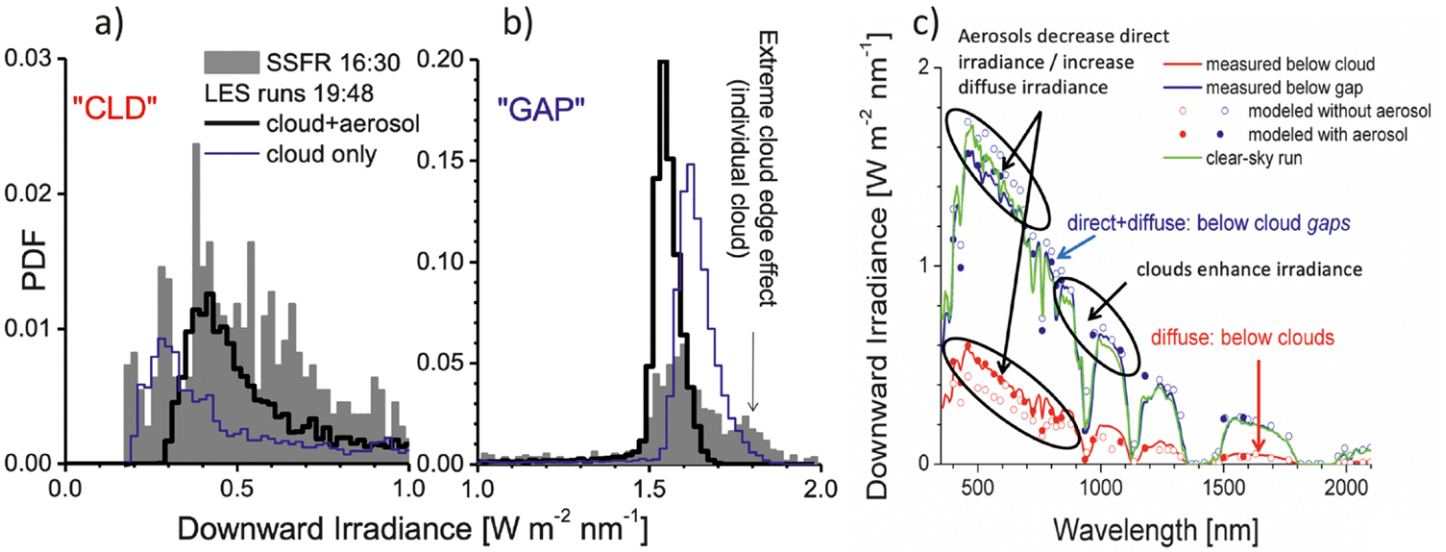


**Fig. 6. Measured (gray) and LES-modeled (black and blue lines) downwelling irradiance below a scattered cloud field at 500 nm: (a) below-cloud mode (CLD) and (b) cloud gap mode (GAP). (c) Location of the two modes as a function of wavelength. Figures adapted from Schmidt et al. (2009). SSFR is the airborne Solar Spectral Flux Radiometer.**

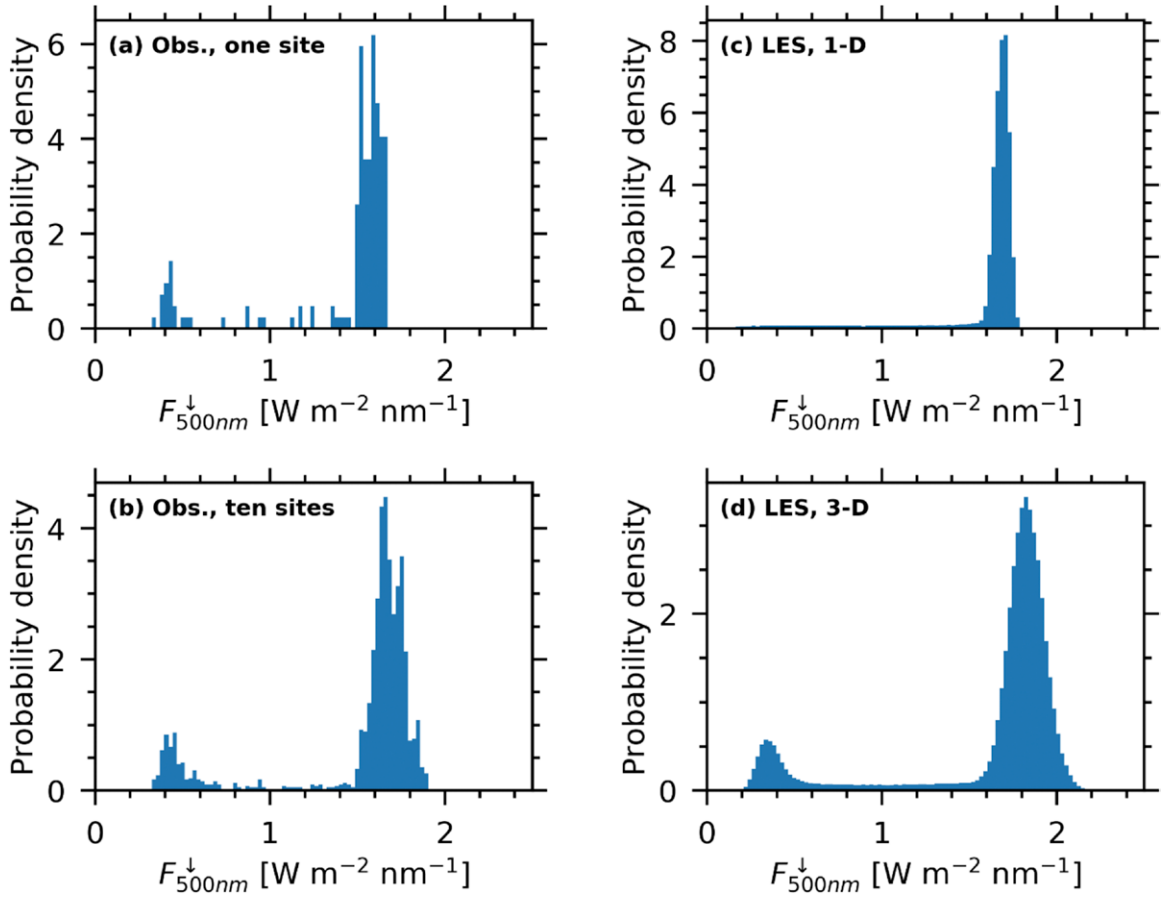


**Fig. 7. (left) PDFs of surface downwelling irradiance at 500 nm ($F^{\downarrow}_{500\,nm}$) from 1400 to 1500 local time (UTC – 5 h) 17 Jul 2017 at the ARM SGP atmospheric observatory. MFRSR observations are taken from (a) the SGP central facility and (b) averaged over 10 surrounding extended facilities (C1, E9, E11, E15, E31, E32, E33, E34, E36, E37). (right) LES output from the same day using the System for Atmospheric Modeling (SAM; Khairoutdinov and Randall 2003) with a 24 km × 24 km domain initialized and forced by observed conditions at SGP is ingested into Monte Carlo radiative transfer to compute $F^{\downarrow}_{500\,nm}$ applying (c) 1D radiative transfer and (d) 3D radiative transfer. Note the variable scales of the vertical axes.**

as horizontally homogeneous layers, does not capture the bimodal PDF at 500 nm (Fig. 7c); however, three-dimensional (3D) RT, which includes vertical and horizontal structure for the identical cloud field, reveals bimodality (Fig. 7d) also captured by the spatially distributed measurements (Fig. 7b).

Gristey et al. (2020) showed that neglecting 3D radiative effects in 1D radiative transfer calculations also introduces a bias of 2–8 W $m^{-2}$ in calculated broadband surface solar irradiance under shallow cumulus conditions that persists even with spatiotemporal averaging. The asymptotic 3D bias was found to be between 2 and 8 W $m^{-2}$ for the cases considered. As such, neglecting 3D radiative effects may cause erroneous surface energy budget calculations even within large-scale weather and climate models as well as lead to incorrect dynamical feedbacks (e.g., Jakub and Mayer 2017; Gronemeier et al. 2017). Quantifying the significance of these effects and determining how they can be accounted for in numerical models considering both accuracy and computational efficiency is an area of active research.

One of the strengths of the PDF-based approach is that closure between microphysical properties of the cloud field from LES and the radiation field from measurements (Fig. 6) is achieved when the location and shape of the two modes is accurately reproduced by the 3D RT model—even if the ratio of the area between the two modes (a measure of cloud fraction) and thus the domain-average irradiance are *not* reproduced. Defined in this way, 3D radiative closure, is less stringent than 1D radiative closure that does require agreement of domain-average modeled and measured irradiance. Separate bookkeeping for the primary contributing modes as shown in Fig. 6 makes this type of closure viable for surface- and aircraft-based studies of cloud radiative effects. That is because it is less sensitive to an accurate representation of the cloud fraction in the modeled cloud field, which can be difficult to achieve.

Because of this separate bookkeeping of clear and cloudy modes in 3D radiative closure, it is also possible to disentangle aerosol and cloud radiative effects in mixed scenes with broken clouds. In terms of the *mean* downwelling irradiance, aerosols would be hard to detect in such situations because their radiative effects produce small perturbations relative to the cloud radiative effects. However, as can be seen in Fig. 6a versus Fig. 6b, aerosols perturb the primary modes of a broken cloud field in different ways, and that is what makes aerosols detectable, even when accompanied by broken clouds that dominate the cloud–aerosol radiative effect. Plotting the location of the two modes spectrally (Fig. 6c) makes this even more obvious. Spectral observations enable not only the detection, but also the quantification of aerosol radiative effects in the context of broken clouds. Broadband observations cannot deliver on this task because they aggregate the spectrum, masking the distinct spectral dependence of the aerosol radiative effect in the cloud and between-cloud observations. To quantify aerosol and cloud radiative effects separately for this application, the absorption features of water vapor (e.g., at 936 nm in Fig. 6c) and other gases must be resolved to avoid aliasing/biasing their radiative effects. Spectroradiometers also must cover sufficient range to capture the aerosol optical thickness spectral dependence.

## Conclusions

New observational tools are needed to tackle the challenges of improving and evaluating the climate model parameterizations of fine-scale processes that drive cloud and aerosol climate radiative forcing and feedbacks. We have given several examples demonstrating how the SW spectral dimension can reveal novel information to understand cloud microphysical and radiative processes in the Earth's atmosphere. Of particular note is the disambiguating nature of these observations: where atmospheric processes of interest produce a unique spectral signature, the spectral observations provide a level of insight into that process that would

otherwise be unclear with broadband observations. We show how a number of effects can be disentangled simultaneously with the distinguishing capabilities of the ground-based SW spectral measurements due to high temporal resolution and a ground-based viewing geometry. Still, the record of SW hyperspectral measurements at U.S. DOE ARM sites has only been analyzed superficially. Within the long-term record, we expect that the potential of SW spectral measurements to better quantify and separate the feedbacks of aerosol, clouds, and 3D effects has only begun to be explored.

**Acknowledgments.** Support for the work described in this article was provided by the U.S. DOE ARM and Atmospheric System Research (ASR) programs.

**Data availability statement.** All data discussed in this article are freely available from www.arm.gov as cited in Table 1.

## References


Alexandrov, M. D., A. A. Lacis, B. E. Carlson, and B. Cairns, 2002a: Remote sensing of atmospheric aerosols and trace gases by means of multifilter rotating shadowband radiometer. Part I: Retrieval algorithm. *J. Atmos. Sci.*, **59**, 524–543, https://doi.org/10.1175/1520-0469(2002)059<0524:RSOAAA>2.0.CO;2.

——, ——, ——, and ——, 2002b: Remote sensing of atmospheric aerosols and trace gases by means of multifilter rotating shadowband radiometer. Part II: Climatological applications. *J. Atmos. Sci.*, **59**, 544–566, https://doi.org/10.1175/1520-0469(2002)059<0544:RSOAAA>2.0.CO;2.

——, and Coauthors, 2009: Columnar water vapor retrievals from multifilter rotating shadowband radiometer data. *J. Geophys. Res.*, **114**, D02306, https://doi.org/10.1029/2008JD010543.

ARM, 2019: Multifilter Rotating Shadowband Radiometer (MFRSR): Southern Great Plains (SGP). ARM Data Center, accessed 26 August 2019, https://doi.org/10.5439/1023898.

Barnard, J. C., C. N. Long, E. I. Kassianov, S. A. McFarlane, J. M. Comstock, M. Freer, and G. M. McFarquhar, 2008: Development and evaluation of a simple algorithm to find cloud optical depth with emphasis on thin ice clouds. *Open Atmos. Sci. J.*, **2**, 46–55, https://doi.org/10.2174/1874282300802010046.

Bar-Or, R. Z., I. Koren, and O. Altaratz, 2010: Estimating cloud field coverage using morphological analysis. *Environ. Res. Lett.*, **5**, 014022, https://doi.org/10.1088/1748-9326/5/1/014022.

Berk, A., and Coauthors, 2006: MODTRAN5: 2006 update. *Proc. SPIE*, **6233**, https://doi.org/10.1117/12.665077.

Bony, S., and J.-L. Dufresne, 2005: Marine boundary layer clouds at the heart of tropical cloud feedback uncertainties in climate models. *Geophys. Res. Lett.*, **32**, L20806, https://doi.org/10.1029/2005GL023851.

Boutle, I. A., S. J. Abel, P. G. Hill, and C. J. Morcrette, 2014: Spatial variability of liquid cloud and rain: Observations and microphysical effects. *Quart. J. Roy. Meteor. Soc.*, **140**, 583–594, https://doi.org/10.1002/qj.2140.

Cess, R. D., and Coauthors, 1990: Intercomparison and interpretation of climate feedback processes in 19 atmospheric general circulation models. *J. Geophys. Res.*, **95**, 16601–16615, https://doi.org/10.1029/JD095iD10p16601.

Chiu, J. C., A. Marshak, Y. Knyazikhin, W. J. Wiscombe, H. W. Barker, J. C. Barnard, and Y. Luo, 2006: Remote sensing of cloud properties using ground-based measurements of zenith radiance. *J. Geophys. Res.*, **111**, D16201, https://doi.org/10.1029/2005JD006843.

——, C. Huang, A. Marshak, I. Slutsker, D. M. Giles, B. N. Holben, Y. Knyazikhin, and W. J. Wiscombe, 2010: Cloud optical depth retrievals from the Aerosol Robotic Network (AERONET) cloud mode observations. *J. Geophys. Res.*, **115**, D14202, https://doi.org/10.1029/2009JD013121.

——, and Coauthors, 2012: Cloud droplet size and liquid water path retrievals from zenith radiance measurements: Examples from the atmospheric radiation measurement program and the aerosol robotic network. *Atmos. Chem. Phys.*, **12**, 10313–10329, https://doi.org/10.5194/acp-12-10313-2012.

Dubovik, O., and M. D. King, 2000: A flexible inversion algorithm for retrieval of aerosol optical properties from Sun and sky radiance measurements. *J. Geophys. Res.*, **105**, 20673–20696, https://doi.org/10.1029/2000JD900282.

Ellingson, R. G., R. D. Cess, and G. L. Potter, 2016: The atmospheric radiation measurement program: Prelude. *The Atmospheric Radiation Measurement (ARM) Program: The First 20 Years, Meteor. Monogr.*, No. 57, Amer. Meteor. Soc., https://doi.org/10.1175/AMSMONOGRAPHS-D-15-0029.1.

Feingold, G., A. McComiskey, T. Yamaguchi, J. S. Johnson, K. S. Carslaw, and K. S. Schmidt, 2016: New approaches to quantifying aerosol influence on the cloud radiative effect. *Proc. Natl. Acad. Sci. USA*, **113**, 5812–5819, https://doi.org/10.1073/pnas.1514035112.

Fielding, M. D., J. C. Chiu, R. J. Hogan, and G. Feingold, 2014: A novel ensemble method for retrieving properties of warm cloud in 3-D using ground-based scanning radar and zenith radiances. *J. Geophys. Res. Atmos.*, **119**, 10912–10930, https://doi.org/10.1002/2014JD021742.

——, ——, ——, ——, E. Eloranta, E. J. O'Connor, and M. P. Cadeddu, 2015: Joint retrievals of cloud and drizzle in marine boundary layer clouds using ground-based radar, lidar and zenith radiances. *Atmos. Meas. Tech.*, **8**, 2663–2683, https://doi.org/10.5194/amt-8-2663-2015.

Ge, J. M., J. Su, T. P. Ackerman, Q. Fu, J. P. Huang, and J. S. Shi, 2010: Dust aerosol optical properties retrieval and radiative forcing over Northwestern China during the 2008 China-US joint field experiment. *J. Geophys. Res.*, **115**, D00K12, https://doi.org/10.1029/2009JD013263.

Giles, D. M., and Coauthors, 2019: Advancements in the Aerosol Robotic Network (AERONET) Version 3 database – Automated near-real-time quality control algorithm with improved cloud screening for Sun photometer aerosol optical depth (AOD) measurements. *Atmos. Meas. Tech.*, **12**, 169–209, https://doi.org/10.5194/amt-12-169-2019.

Gristey, J. J., G. Feingold, I. B. Glenn, K. S. Schmidt, and H. Chen, 2020: Surface solar irradiance in continental shallow cumulus fields: Observations and large eddy simulation. *J. Atmos. Sci.*, **77**, 1065–1080, https://doi.org/10.1175/JAS-D-19-0261.1.

Gronemeier, T., F. Kanani-Sühring, and S. Raasch, 2017: Do shallow cumulus clouds have the potential to trigger secondary circulations via shading? *Bound.-Layer Meteor.*, **162**, 143–169, https://doi.org/10.1007/s10546-016-0180-7.

Gustafson, W. I., and Coauthors, 2020: The Large-Eddy Simulation (LES) Atmospheric Radiation Measurement (ARM) Symbiotic Simulation and Observation (LASSO) activity for continental shallow convection. *Bull. Amer. Meteor. Soc.*, **101**, E462–E479, https://doi.org/10.1175/BAMS-D-19-0065.1.

Harrison, L., and J. Michalsky, 1994: Objective algorithms for the retrieval of optical depths from ground-based measurements. *Appl. Opt.*, **33**, 5126–5132, https://doi.org/10.1364/AO.33.005126.

——, ——, and J. Berndt, 1994: Automated multifilter rotating shadow-band radiometer: An instrument for optical depth and radiation measurements. *Appl. Opt.*, **33**, 5118–5125, https://doi.org/10.1364/AO.33.005118.

Holben, B. N., and Coauthors, 1998: AERONET: A federated instrument network and data archive for aerosol characterization. *Remote Sens. Environ.*, **66**, 1–16, https://doi.org/10.1016/S0034-4257(98)00031-5.

IPCC, 2013: Climate Change 2013: *The Physical Science Basis*. Cambridge University Press, 1535 pp.

Jakub, F., and B. Mayer, 2017: The role of 1-D and 3-D radiative heating in the organization of shallow cumulus convection and the formation of cloud streets. *Atmos. Chem. Phys.*, **17**, 13317–13327, https://doi.org/10.5194/acp-17-13317-2017.

Kassianov, E. I., J. C. Barnard, and T. P. Ackerman, 2005: Retrieval of aerosol microphysical properties using surface Multifilter Rotating Shadowband Radiometer (MFRSR) data: Modeling and observations. *J. Geophys. Res.*, **110**, D09201, https://doi.org/10.1029/2004JD005337.

——, C. J. Flynn, T. P. Ackerman, and J. C. Barnard, 2007: Aerosol single-scattering albedo and asymmetry parameter from MFRSR observations during the ARM Aerosol IOP 2003. *Atmos. Chem. Phys.*, **7**, 3341–3351, https://doi.org/10.5194/acp-7-3341-2007.

——, J. C. Barnard, L. K. Berg, C. Flynn, and C. N. Long, 2011a: Sky cover from MFRSR observations. *Atmos. Meas. Tech.*, **4**, 1463–1470, https://doi.org/10.5194/amt-4-1463-2011.

——, ——, ——, C. N. Long, and C. Flynn, 2011b: Shortwave spectral radiative forcing of cumulus clouds from surface observations. *Geophys. Res. Lett.*, **38**, L07801, https://doi.org/10.1029/2010GL046282.

——, ——, C. Flynn, L. Riihimaki, J. Michalsky, and G. Hodges, 2014: Areal-averaged spectral surface albedo from ground-based transmission data alone: Toward an operational retrieval. *Atmosphere*, **5**, 597–621, https://doi.org/10.3390/atmos5030597.

——, ——, ——, ——, L. K. Berg, and D. A. Rutan, 2017: Areal-averaged spectral surface albedo in an Atlantic coastal area: Estimation from ground-based transmission. *Atmosphere*, **8**, 123, https://doi.org/10.3390/atmos8070123.

Khairoutdinov, M. F., and D. A. Randall, 2003: Cloud resolving modeling of the ARM summer 1997 IOP: Model formulation, results, uncertainties, and

sensitivities. *J. Atmos. Sci.*, **60**, 607–625, https://doi.org/10.1175/1520-0469(2003)060<0607:CRMOTA>2.0.CO;2.

Klein, S. A., and A. Hall, 2015: Emergent constraints for cloud feedbacks. *Curr. Climate Change Rep.*, **1**, 276–287, https://doi.org/10.1007/s40641-015-0027-1.

Kollias, P., and Coauthors, 2020: The ARM radar network: At the leading edge of cloud and precipitation observations. *Bull. Amer. Meteor. Soc.*, **101**, E588–E607, https://doi.org/10.1175/BAMS-D-18-0288.1.

Koren, I., L. A. Remer, Y. J. Kaufman, Y. Rudic, and J. V. Martins, 2007: On the twilight zone between clouds and aerosols. *Geophys. Res. Lett.*, **34**, L08805, https://doi.org/10.1029/2007GL029253.

——, G. Feingold, H. Jiang, and O. Altaratz, 2009: Aerosol effects on the inter-cloud region of a small cumulus cloud field. *Geophys. Res. Lett.*, **36**, L14805, https://doi.org/10.1029/2009GL037424.

LeBlanc, S. E., P. Pilewskie, K. S. Schmidt, and O. Coddington, 2015: A spectral method for discriminating thermodynamic phase and retrieving cloud optical thickness and effective radius using transmitted solar radiance spectra. *Atmos. Meas. Tech.*, **8**, 1361–1383, https://doi.org/10.5194/amt-8-1361-2015.

Lu, M.-L., G. Feingold, H. H. Jonsson, P. Y. Chuang, H. Gates, R. C. Flagan, and J. H. Seinfeld, 2008: Aerosol-cloud relationships in continental shallow cumulus. *J. Geophys. Res.*, **113**, D15201, https://doi.org/10.1029/2007JD009354.

Lubin, D., and A. M. Vogelmann, 2011: The influence of mixed-phase clouds on surface shortwave irradiance during the Arctic spring. *J. Geophys. Res.*, **116**, D00T05, https://doi.org/10.1029/2011JD015761.

Mace, G. G., S. Avey, S. Cooper, M. Lebsock, S. Tanelli, and G. Dobrowalski, 2016: Retrieving co-occurring cloud and precipitation properties of warm marine boundary layer clouds with A-Train data. *J. Geophys. Res. Atmos.*, **121**, 4008–4033, https://doi.org/10.1002/2015JD023681.

Marshak, A., Y. Knyazikhin, K. D. Evans, and W. J. Wiscombe, 2004: The "RED versus NIR" plane to retrieve broken-cloud optical depth from ground-based measurements. *J. Atmos. Sci.*, **61**, 1911–1925, https://doi.org/10.1175/1520-0469(2004)061<1911:TRVNPT>2.0.CO;2.

McBride, P. J., K. S. Schmidt, P. Pilewskie, A. S. Kittelman, and D. E. Wolfe, 2011: A spectral method for retrieving cloud optical thickness and effective radius from surface-based transmittance measurements. *Atmos. Chem. Phys.*, **11**, 7235–7252, https://doi.org/10.5194/acp-11-7235-2011.

McComiskey, A., and R. A. Ferrare, 2016: Aerosol physical and optical properties in the ARM Program. *The Atmospheric Radiation Measurement (ARM) Program: The First 20 Years, Meteor. Monogr.*, No. 57, Amer. Meteor. Soc., https://doi.org/10.1175/AMSMONOGRAPHS-D-15-0028.1.

——, S. E. Schwartz, B. Schmid, H. Guan, E. R. Lewis, P. Ricchiazzi, and J. A. Ogren, 2008: Direct aerosol forcing: Calculation from observables and sensitivities to inputs. *J. Geophys. Res.*, **113**, D09202, https://doi.org/10.1029/2007JD009170.

Michalsky, J. J., and C. N. Long, 2016: ARM solar and infrared broadband and filter radiometry. *The Atmospheric Radiation Measurement (ARM) Program: The First 20 Years, Meteor. Monogr.*, No. 57, Amer. Meteor. Soc., https://doi.org/10.1175/AMSMONOGRAPHS-D-15-0031.1.

——, J. C. Liljegren, and L. C. Harrison, 1995: A comparison of Sun photometer derivations of total column water vapor and ozone to standard measures of same at the Southern Great Plains Atmospheric Radiation Measurement site. *J. Geophys. Res.*, **100**, 25 995–26 003, https://doi.org/10.1029/95JD02706.

——, F. Denn, C. Flynn, G. Hodges, P. Kiedron, A. Koontz, J. Schlemmer, and S. E. Schwartz, 2010: Climatology of aerosol optical depth in north central Oklahoma: 1992–2008. *J. Geophys. Res.*, **115**, D07203, https://doi.org/10.1029/2009JD012197.

Min, Q., and L. C. Harrison, 1996: Cloud properties derived from surface MFRSR measurements and comparison with GOES results at the ARM SGP site. *Geophys. Res. Lett.*, **23**, 1641–1644, https://doi.org/10.1029/96GL01488.

——, T. Wang, C. N. Long, and M. Duan, 2008: Estimating fractional sky cover from spectral measurements. *J. Geophys. Res.*, **113**, D20208, https://doi.org/10.1029/2008JD010278.

Mlawer, E. J., and D. D. Turner, 2016: Spectral radiation measurements and analysis in the ARM Program. *The Atmospheric Radiation Measurement (ARM) Program: The First 20 Years, Meteor. Monogr.*, No. 57, Amer. Meteor. Soc., https://doi.org/10.1175/AMSMONOGRAPHS-D-15-0027.1.

——, M. J. Iacono, R. Pincus, H. W. Barker, L. Oreopoulos, and D. L. Mitchell, 2016: Contributions of the ARM program to radiative transfer modeling for climate and weather applications. *The Atmospheric Radiation Measurement (ARM) Program: The First 20 Years, Meteor. Monogr.*, No. 57, Amer. Meteor. Soc., https://doi.org/10.1175/AMSMONOGRAPHS-D-15-0041.1.

Nam, C., S. Bony, J.-L. Dufresne, and H. Chepfer, 2012: The 'too few, too bright' tropical low-cloud problem in CMIP5 models. *Geophys. Res. Lett.*, **39**, L21801, https://doi.org/10.1029/2012GL053421.

Nicolas, J. P., and Coauthors, 2017: January 2016 extensive summer melt in West Antarctica favoured by strong El Nino. *Nat. Commun.*, **8**, 15799, https://doi.org/10.1038/ncomms15799.

Pinsky, M., and A. P. Khain, 2018: Theoretical analysis of the entrainment–mixing process at cloud boundaries. Part I: Droplet size distributions and humidity within the interface zone. *J. Atmos. Sci.*, **75**, 2049–2064, https://doi.org/10.1175/JAS-D-17-0308.1.

Schmidt, K. S., V. Venema, F. Di Giuseppe, R. Scheirer, M. Wendisch, and P. Pilewskie, 2007: Reproducing cloud microphysical and irradiance measurements using three 3D cloud generators. *Quart. J. Roy. Meteor. Soc.*, **133**, 765–780, https://doi.org/10.1002/qj.53.

——, G. Feingold, P. Pilewskie, H. Jiang, O. Coddington, and M. Wendisch, 2009: Irradiance in polluted cumulus fields: Measured and modeled cloud-aerosol effects. *Geophys. Res. Lett.*, **36**, L07804, https://doi.org/10.1029/2008GL036848.

Scott, R. C., and D. Lubin, 2014: Mixed-phase cloud radiative properties over Ross Island, Antarctica: The influence of various synoptic-scale atmospheric circulation regimes. *J. Geophys. Res. Atmos.*, **119**, 6702–6723, https://doi.org/10.1002/2013JD021132.

Slingo, A., 1989: A GCM parameterization for the shortwave radiative properties of water clouds. *J. Atmos. Sci.*, **46**, 1419–1427, https://doi.org/10.1175/1520-0469(1989)046<1419:AGPFTS>2.0.CO;2.

Stephens, G. L., and Coauthors, 2010: Dreary state of precipitation in global models. *J. Geophys. Res.*, **115**, D24211, https://doi.org/10.1029/2010JD014532.

——, and Coauthors, 2012: An update on Earth's energy balance in light of the latest global observations. *Nat. Geosci.*, **5**, 691–696, https://doi.org/10.1038/ngeo1580.

Stokes, G. M., 2016: Original ARM concept and launch. *The Atmospheric Radiation Measurement (ARM) Program: The First 20 Years, Meteor. Monogr.*, No. 57, Amer. Meteor. Soc., https://doi.org/10.1175/AMSMONOGRAPHS-D-15-0021.1.

Turner, D. D., E. J. Mlawer, and H. E. Revercomb, 2016: Water vapor observations in the ARM Program. *The Atmospheric Radiation Measurement (ARM) Program: The First 20 Years, Meteor. Monogr.*, No. 57, Amer. Meteor. Soc., https://doi.org/10.1175/AMSMONOGRAPHS-D-15-0025.1.

Uin, J., and Coauthors, 2019: Atmospheric Radiation Measurement (ARM) Aerosol Observing Systems (AOS) for surface-based in-situ atmospheric aerosol and trace gas measurements. *J. Atmos. Oceanic Technol.*, **36**, 2429–2447, https://doi.org/10.1175/JTECH-D-19-0077.1.

Varnai, T., and A. Marshak, 2011: Global CALIPSO observations of aerosol changes near clouds. *IEEE Geosci. Remote Sens. Lett.*, **8**, 19–23, https://doi.org/10.1109/LGRS.2010.2049982.

Wielicki, B. A., and Coauthors, 2013: Achieving climate change absolute accuracy in orbit. *Bull. Amer. Meteor. Soc.*, **94**, 1519–1539, https://doi.org/10.1175/BAMS-D-12-00149.1.

Wilson, A., R. C. Scott, M. P. Cadeddu, V. Ghate, and D. Lubin, 2018: Cloud optical properties over West Antarctica from shortwave spectroradiometer measurements during AWARE. *J. Geophys. Res. Atmos.*, **123**, 9559–9570, https://doi.org/10.1029/2018JD028347.

Yang, W., and Coauthors, 2016: Observation of the spectrally invariant properties of clouds in cloudy-to-clear transition zones during the MAGIC field campaign. *Atmos. Res.*, **182**, 294–301, https://doi.org/10.1016/j.atmosres.2016.08.004.

——, A. Marshak, and G. Wen, 2019: Cloud edge properties measured by the ARM shortwave spectrometer over ocean and land. *J. Geophys. Res. Atmos.*, **124**, 8707–8721, https://doi.org/10.1029/2019JD030622.